Available online at www.sciencedirect.com
ScienceDirect
Acta Materialia 56 (2008) 4002–4011
Acta MATERIALIA
www.elsevier.com/locate/actamat

Origin of intragranular crystallographic misorientations in hot-dip Al–Zn–Si coatings

Ch. Niederberger [a,b], J. Michler [b], A. Jacot [a,*]

[a] Computational Materials Laboratory, Institute of Materials, Ecole Polytechnique Fédérale de Lausanne, Station 12, CH-1015 Lausanne, Switzerland
[b] Laboratory for Mechanics of Materials and Nanostructures, EMPA, Swiss Federal Laboratories for Materials Testing and Research, Feuerwerkerstrasse 39, CH-3602 Thun, Switzerland

Received 21 December 2007; received in revised form 15 April 2008; accepted 15 April 2008
Available online 22 May 2008

Abstract

The origin of intragranular variations of the crystallographic orientation in hot-dip Al–Zn–Si coatings is discussed based on new experimental results and modelling. The solidification microstructure in as-received 55Al–43.4Zn–1.6Si (in wt.%) coatings deposited on steel plates in an industrial production line was analyzed by electron backscattered diffraction, glow-discharge optical emission spectroscopy and atomic force microscopy (AFM). The results were compared with those obtained in coatings re-solidified under different cooling and mechanical loading conditions. Continuous variations of the crystallographic orientation as large as 35° were observed within individual grains of Al–Zn–Si, consistent with previous studies. However, the mechanisms previously proposed for the origin of intragranular crystallographic misorientations had to be revisited. The new experimental data acquired during this study indicate that the solidification shrinkage accumulating in the area of the grain envelope is the driving force for the formation of intragranular misorientations. The solidification shrinkage leads to the development of tensile stresses in the oxide film covering the coating while it solidifies. Estimations based on AFM profiles and phase field simulations of the dendritic structure indicate that the stresses applied on the dendrite network are sufficient to deform plastically the dendrite arms during solidification.

Keywords: Solidification microstructures; Al–Zn; Hot-dipping; Crystallographic misorientations; Solidification shrinkage

1. Introduction

Variations of the crystallographic orientation within a given grain are relatively common in solidification microstructures. In some cases, such intragranular misorientations can affect the properties and performance of the final component. The single-crystal turbine blades made of Ni-base superalloys, which are used in the first stages of aeronautic and land-based gas turbines, are a typical example. In these single grain components variations of the crystallographic orientation by 5–10° and low-angle boundaries are commonly observed between the bottom and the top of the blade, which has a detrimental effect on the mechanical properties by facilitating creep through diffusion in subgrain boundaries. Another alloy system in which substantial intragranular misorientations were discovered recently are Al–Zn–Si coatings deposited on steel by hot-dipping, where misorientations reaching 35° have been reported across individual grains [1]. Both in superalloys and Al–Zn–Si coatings, literature about the formation of intragranular crystallographic misorientations and the mechanisms at the origin of it is rather scarce and can be shortly reviewed as follows. In one of the first studies devoted to this topic, Rappaz and Blank observed the formation of layered misorientation structures in Ni-based single-crystal castings [2]. They found that the orientation is essentially constant within individual dendrites and rows of dendrites, whereas it can vary by a few degrees between adjacent rows of dendrites. The authors related the misorientations to branching events during solidification. In 1989, Agapova et al. reported that the overall shape of

* Corresponding author. Tel.: +41 21 693 4798; fax: +41 21 693 5890.
E-mail address: alain.jacot@epfl.ch (A. Jacot).

1359-6454/$34.00 © 2008 Acta Materialia Inc. Published by Elsevier Ltd. All rights reserved.
doi:10.1016/j.actamat.2008.04.037

the solidification front, which is dictated by the heat flow in the process, is an important factor for the formation of low-angle boundaries [3]. Paul et al. [4] correlated the relatively large liquid undercooling ahead of the growth front in the platform region of single-crystal turbine blades with distortions of the crystal lattice. Siredey et al. [5] emphasized that misorientations were already present at early stages of growth, namely at the end of the grain selector, and deteriorates as growth proceeds, leading to more pronounced but random misorientations in the upper part of a single-crystal casting. They tentatively proposed that the observed misorientations are due to thermomechanical stresses which build up during γ' precipitation, which takes place only slightly below the solidus temperature in the studied alloy. Napolitano and Schaefer [6] proposed a mechanism for the formation of low-angle boundaries in the platform region of a turbine blade where the envelope of the solidification front splits into two parts before forming a low-angle boundary where they join higher in the casting. Recent studies using the electron backscattered diffraction (EBSD) technique led to a more detailed picture of the misorientations in cast single-crystal turbine blades. By studying CMSX4 and CMSX10N castings, Newell et al. [7] found that under steady state growth conditions misorientations of random nature occur and can reach a magnitude of about 2°. In the platform area, however, they observed continuous and cumulative misorientations of up to 6°. They associated these misorientations with the fact that the undercooling is higher in this area, which leads to a larger dendrite tip velocity and a finer dendritic network. D'Souza et al. [8], who also studied misorientations in the platform region of blade castings, suggested that the cumulative misorientations are due to contraction stresses resulting in plastic bending of the dendrite arms at intermediate solid fractions. The low-angle boundaries are subsequently produced when the independently advancing growth fronts converge as proposed by Napolitano and Schaefer [6]. Another interesting observation of misorientations in Ni-based single crystals has been made by Wagner et al. [9], who analyzed quenched castings during directional solidification. In the zones of extremely rapid growth ahead of the quenched dendritic front, they found very significant, continuous and cumulative misorientations as large as 20°. They suggested that these misorientations are due to thermomechanical stresses arising from the outer shell of the casting, which solidifies quickly during quenching. These stresses may lead to the deformation of the very fine dendrite structure in the core of the casting.

Low-angle boundaries have also been reported in other systems such as single-crystal solidification of Mo–Re alloys [10] and Cu alloys [11,12]. In the latter two references it was shown that crystallographic misorientations can arise from mechanical deformation of dendrites through fluid flow in the mushy zone. However, this effect becomes important only at very high undercoolings where the dendrite structure is very fine and where growth velocity and fluid flow are very important.

Sémoroz et al. [1,13] reported intragranular variations of the crystallographic orientation in Al–Zn–Si and Zn–Al alloy coatings deposited on steel substrates by hot-dipping. Their study is of particular interest as misorientations as large as 35° are observed in the coarse-grained coating layers, whereas misorientations of only a couple of degrees are normally observed in Ni-base single-crystal castings. This makes the Al–Zn–Si and Zn–Al coating systems particularly suitable in order to study the mechanisms involved in the formation of misorientations. Two possible mechanisms have been proposed by Sémoroz et al. [1,13]. The first one is associated with the thermomechanical stresses that develop during cooling due to differential thermal contraction in the substrate–coating composite. Since the substrate is much more rigid than the coating due to its thickness and composition, the differences of thermal strain are essentially accommodated by the coating, which will undergo plastic deformation under tension and can possibly accumulate geometrically necessary dislocations. The second hypothesis is associated with the microsegregation of Zn from the core to the periphery of the dendrite arms, which is expected to be very pronounced due to the morphology of the phase diagram. As the lattice parameter of the Al–Zn solid solution decreases for increasing Zn content, systematic misorientations could develop by distortion of the crystal lattice. The typical misorientation rates that can be expected for the thermomechanical and microsegregation hypotheses were analyzed and it was concluded that rates of $5° \text{ mm}^{-1}$ are realistic for both mechanisms [1,13].

The objective of this contribution is to bring a better answer to the question of the origin of misorientations in hot-dip Al–Zn–Si coatings by performing a detailed characterization of coatings that have solidified under different mechanical conditions. The coatings are characterized in terms of microstructure, crystallographic misorientations, chemistry (microsegregation) and topography. Based on these results, a new mechanism is proposed to explain the development of misorientations in hot-dip Al–Zn–Si coatings.

2. Experimental

The analyzed material is a 55Al–43.4Zn–1.6Si (in wt.%) coating deposited on 1 mm thick steel plates in the industrial production line of BHP steel (today BlueScope Steel). The crystallographic orientations in the coating in the as-received state were analyzed by electron backscatter diffraction (EBSD). The samples for EBSD analysis were prepared by diamond polishing using 6, 1 and 0.25 μm grits on Struers DP-Mol and DP-Nap cloths, lubricated with red DP lubricant from Struers or ethanol. A subsequent electropolishing step was performed to remove the plastically deformed surface layer. The electropolishing was carried out with a microprocessor-controlled LectroPol-5 apparatus from Struers and an electrolyte consisting of a solution equivalent to Struers A2 or 720 ml ethanol, 200 ml 2-butyloxyethanol ($C_6H_{14}O_2$) and 80 ml perchloric acid ($HClO_4$,

70%). Best results were obtained for an applied voltage of 25 V and a polishing time of 2–3 s. The EBSD measurements were conducted on a Philips XL30 FEG SEM equipped with Nordlys EBSD detector from HKL, using an acceleration voltage of 20 kV. The recorded Pseudo–Kikuchi patterns were treated with a HKL Channel 5 acquisition and data processing software.

Concentration profiles in the direction normal to the coating surface were measured by glow-discharge optical emission spectroscopy (GD-OES) using a JY 5000 RF instrument from Jobin–Yvon Horiba and equipped by a glow-discharge source of 4 mm diameter [14].

The topography of the coating in the as-received state was characterized with a TopoMetrix Explorer TMX 1000 atomic force microscope (AFM). Areas of 100×100 μm and 20×20 μm were scanned with a maximum z-displacement of 12 μm and a lateral resolution of 20 nm. The data were processed with Mountains Map Universal and Matlab software.

Re-solidification experiments have been conducted on the coated material to investigate the influence of the thermomechanical stresses on intragranular misorientations and microstructure. The experiments were performed with an Ulvac–Riko VHT-E48 infrared furnace controlled by an OMRON ES100P console. A coated plate of 15 by 25 mm was placed in a 40 mm diameter quartz tube positioned along the central axis of the furnace. The sample was then heated above the liquidus temperature of the coating alloy (600 °C) and cooled down by a He gas flow at a prescribed rate ranging between 1 and 20 K s^{-1}. The sample was held by two ceramic tubes in which K-type thermocouple wires were inserted. The thermocouples were spot-welded at different positions and on both sides of the sample in order to monitor the temperature gradients. In order to study the influence of the thermomechanical stresses on intragranular misorientations, a sample holder was designed with the objective of reducing the thermomechanical stresses and strains in the coating. The sample holder consisted of two massive plates of CuZn37Pb3 brass which were positioned on both sides of the substrate–coating sample. Being massive, the brass plates impose their thermal expansion to the sample if the system is tightly assembled. The thermal expansion coefficient of brass is much closer to that of Al–Zn–Si than that of steel. Therefore, the stresses in the coating are significantly reduced by the presence of the brass plates. Re-solidification experiments using a loose assembly were also carried out for the sake of comparison. Crystallographic orientation maps of the re-solidified samples were then acquired by EBSD using the same preparation and equipment as described above.

3. Results

3.1. As-deposited samples

Fig. 1 shows an EBSD misorientation map of a large grain in an Al–Zn–Si coating in the as-received state. The reference orientation (0°, blue) was assigned to the nucleation centre of the grain, which was determined by optical microscopy. The colour scale shows that the crystallographic orientation can vary by 16° from the centre to the periphery of the grain, with a rate of about 5° mm^{-1}. This result confirms those reported by Sémoroz et al. [1]. Further investigations by optical microscopy showed that the variation of the crystallographic orientation follows in most cases distinct patterns of the dendritic network. From a careful inspection of the misorientation maps, one can distinguish three different types of intragranular misorientations, which are indicated with black circles in Fig. 1b:

1. Continuous variation of the orientation along a dendrite arm, as it occurs in many areas of Fig. 1a and b, where gradual changes of the colour code are clearly visible.
2. Subgrain boundaries corresponding to sharp orientation changes. Subgrain boundaries appear to be associated with misorientations events that occurred in certain dendrite arms which then transmitted their orientation to the area where they grew. A typical example is the subgrain boundary that is observed near the nucleation centre of the grain (left of Fig. 1b).
3. Misoriented areas of band-like shape that are not directly related to the grain and dendrite structure (labelled 3 in Fig. 1b). Unlike in type 1, the orientation is approximately the same on both sides of the misoriented area. Consequently, this type of misorientation does not contribute to the large orientation variations that are observed between the centre and the periphery of the grain and will not be further discussed here.

Continuous misorientations of type 1 are responsible for a significant part of the misorientations observed in Al–Zn–Si coatings. Fig. 2 shows an EBSD misorientation map taken along a dendrite arm that grew from the left to the right and emitted secondary arms on both sides. As can be seen, the orientation variation is truly continuous, as no sudden misorientation of 1° or more can be identified within the dendrite arm. The rotation axis corresponding to the orientation variations of Fig. 2 and in other grains has been analyzed in Ref. [15]. It was shown that the orientation axis lies in the plane of the coating and is approximately perpendicular to the dendrite growth direction. The sense of the rotation is systematically towards the substrate. The same observation was previously made by Sémoroz et al. [1] and was further confirmed by the inspection of other grains [15].

Fig. 3a shows a metallographic section in the plane of the coating layer where a dendrite arm, which grew from the lower right to the upper left of the picture, is visible. The primary dendrite arm underwent two branching events, which are probably associated with the fact that the dendrite is confined by the free surface. Fig. 3b shows a detailed EBSD map of the area where the first branching event occurred (outlined by a white box in Fig. 3a). It

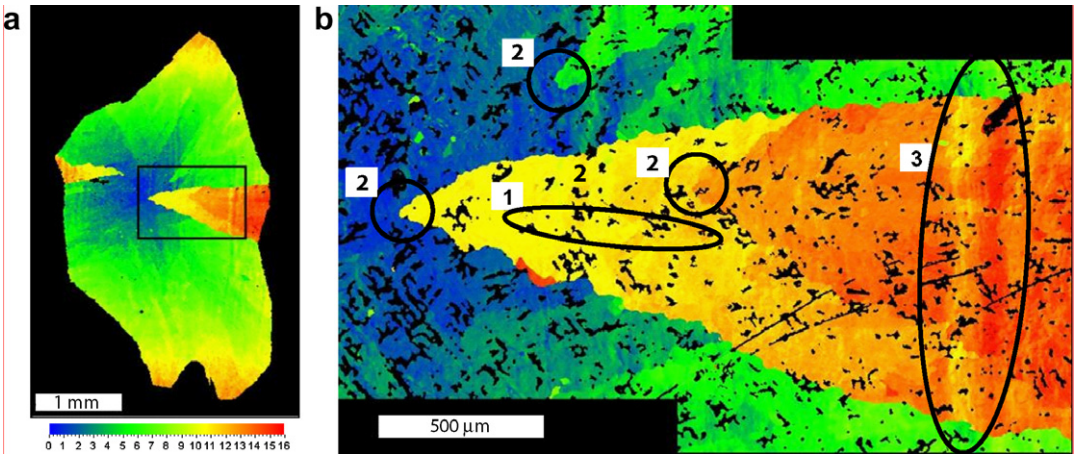

Fig. 1. EBSD misorientation map of a typical grain in an Al–Zn–Si coating (a) and higher resolution mapping (b). The labels in (b) correspond to different kinds of misorientations which are commented on in the text. The reference orientation was taken at the location of the grain nucleus which was identified by optical microscopy.

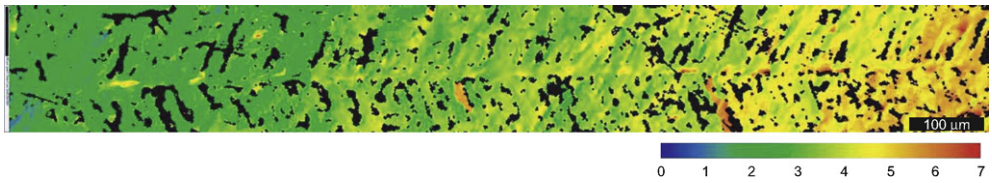

Fig. 2. EBSD misorientation map of an area around a primary dendrite arm (grown from the left).

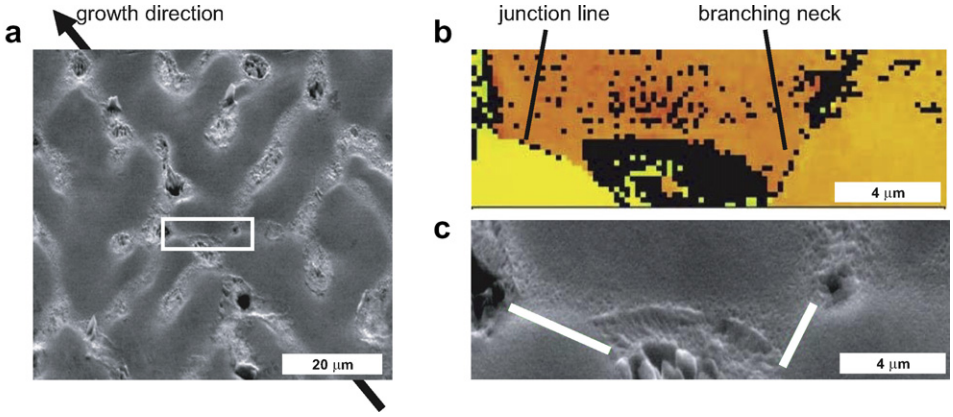

Fig. 3. Secondary electron micrograph of an electropolished coating surface showing the dendrite pattern (a), EBSD misorientation map (b) and secondary electron micrograph (c) of the area corresponding to the white frame in (a). The subgrain boundaries are indicated by thick white lines in (c).

reveals two subgrain boundaries, corresponding to misorientations of about 1° (right) and 2° (left). The right subgrain boundary is located in the branching neck, while the left one is located at a junction line where two neighbouring dendrite arms seem to have coalesced. As in Fig. 2, the misorientation axis is approximately parallel to the plane of the coating and perpendicular to the primary growth direction. This result suggests that repeated misorientations localized in branching necks can be responsible for the cumulative misorientations observed in the coatings.

Fig. 4 shows a typical depth concentration profile measured by GD-OES. It indicates that the concentration is not homogeneous in the Al–Zn–Si coating. Maxima of the Al concentration are observed close to the surface of the coating and near the substrate–coating interface. In the centre and at the very surface of the coating, maxima of the Zn concentration are observed. At the substrate–coating interface, the transition of the concentration profiles appears to be quite smooth. Intermetallic layers which are composed of Fe, Al, Si and Zn are partly responsible for this. Another factor is the relief of the coating surface

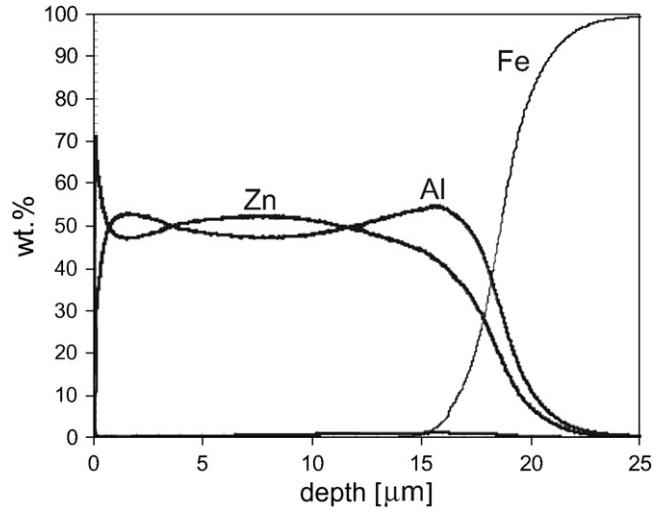

Fig. 4. GD-OES depth profile of the concentration in an as-received Al–Zn–Si coating.

which propagates during the sputtering process. Within the coating, i.e. for a depth smaller than 17 μm, it seems clear, however, that the origin of the concentration differences is microsegregation. The maxima of Al concentration observed in the vicinity of the two boundaries indicate that these are the preferred areas for the growth of the primary α-Al dendrites during the first stage of solidification.

The AFM mapping of the coating surface reveals the details of its topography. Fig. 5a shows an AFM map of a region where two different surface morphologies are present. In the upper half of Fig. 5a, a series of secondary dendrite arms, which are attached to a horizontal primary trunk at the centre of the picture, clearly seem to have grown close to the free surface. In this area the surface has a so-called shiny appearance when observed at larger scale [16]. The lower half of the map corresponds to a grain area where the microstructure is dominated by secondary or tertiary dendrite arms that developed from dendrite trunks growing close to the substrate. After having reached the free surface these secondary or tertiary arms leave behind a structure of hillocks and dimples, which would appear as "dull" in larger-scale observations [16]. Fig. 5b shows a detail AFM map corresponding to the black square drawn in Fig. 5a. The shadowing reveals wrinkles which span over the dimples. They were identified as wrinkles in the oxide skin forming at the surface of the remaining liquid during solidification. This oxide skin underwent compression, which has been attributed to solidification shrinkage [15].

3.2. Re-solidification experiments

Table 1 contains the misorientation rates measured by EBSD in the coating after re-solidification with or without imposing the strain with the brass device. The cooling rate was about 5 K s^{-1} in both cases. The misorientation rates can be compared with those of an industrially produced reference sample. It can be seen that the re-solidified samples exhibit considerably smaller misorientation rates than the industrial sample, whereas the difference between the two re-solidified cases is rather small. Unexpectedly, the sample that was tightly assembled to the brass discs shows a slightly higher misorientation rate than the loose one, but the difference is not significant considering the high standard deviation of the measurements. One can deduce that the modified thermal contraction imposed by the brass setup does not influence significantly the intragranular misorientations. On the other hand the cooling rate during solidification seems to be clearly an important factor for the misorientation rate as the coatings re-solidified at 5 K s^{-1} exhibit considerably smaller misorientation rates than the industrial ones, which were solidified at a cooling rate of approximately 30 K s^{-1}.

Fig. 6 shows a detail of a typical cooling curve as it was measured during re-solidification in the infrared furnace.

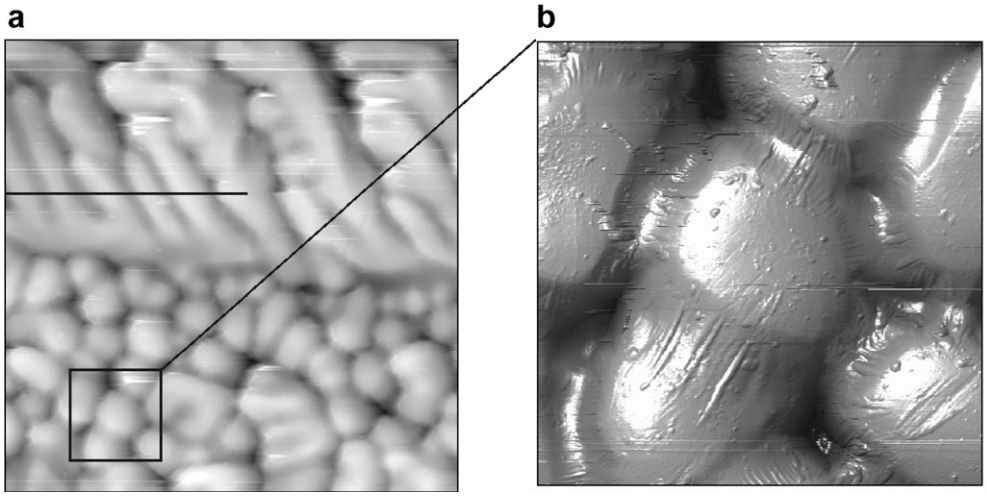

Fig. 5. AFM topography map of a 100 μm × 100 μm area (a) and 20 μm × 20 μm enlargement (b) at the surface of an as-received Al–Zn–Si coating. The applied shadowing reveals oxide wrinkles at the coating surface.

Table 1
Misorientation rates measured in as-received and re-solidified samples

	Number of profiles	Misorientation rate $d\tau/dx$ (° mm^{-1})			
		Minimum	Maximum	Mean	Standard deviation
As-received industrial samples	33	1.62	8.86	4.36	1.55
Re-solidification without imposed strain	36	0.36	3.76	1.86	0.98
Re-solidification with imposed strain	45	0.37	5.49	2.07	1.31

The cooling rate is approximately constant in the solidification interval of the alloy except for a small decrease between 535 and 530 °C. The inflection observed in Fig. 6 corresponds to a time shift, Δt, of about 0.25 s. Since such inflections were systematically detected in all experiments they were interpreted as the latent heat release during the first stage of solidification, when the dendritic network rapidly expands. A heat flow balance can thus be established:

$$\dot{T}\rho c_p\, d_{\text{coated steel}}\Delta t = g_s L\, d_{\text{coating}} \quad (1)$$

where $\dot{T}$ is the cooling rate before and after the inflection, $\rho c_p = 3.8 \times 10^6$ J m^{-3} K^{-1} is the volumetric specific heat of the plate, $d_{\text{coated steel}} = 0.5$ mm is the thickness of the coated plate, $L = 9 \times 10^8$ J m^{-3} is the volumetric latent heat of fusion of the coating alloy, $d_{\text{coating}} = 20$ μm is the thickness of the coating, and g_s is the volume fraction of solid at the end of the inflection. Extracting g_s from the above equation yields about $g_s = 0.33$ for the end of the inflection visible in Fig. 6. The analysis was repeated on several samples and it was found that a solid fraction of about 1/3 is well reproducible. The end of the inflection can be associated with the moment when most of the dendrite tips sustaining the grain envelopes have impinged with boundaries or neighbouring grains. Beyond that point, solidification proceeds more slowly by thickening of existing dendrite arms. The release of latent heat becomes very difficult to extract from the cooling curve owing to the slower solidification rate and the high heat capacity of the steel substrate.

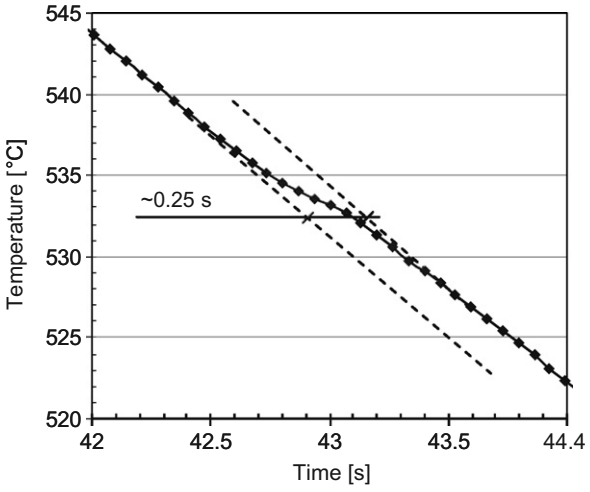

Fig. 6. Typical temperature evolution measured during re-solidification. The cooling rate (here 12.5 K s^{-1}) is constant in the solidification interval except for a sudden decrease between 535 and 530 °C, which is due to the release of latent heat during the formation of the dendritic network.

Considering that the liquidus temperature of the coating alloy at the nominal composition of Al–43.4 wt.% Zn–1.6 wt.% Si is about 564 °C [17], the first stage of solidification appears to take place at very large growth undercooling. However, the actual growth undercooling is most probably much lower than 30 K, as $FeAl_3$ and Fe_2Al_5 intermetallic layers at the coating/substrate interface thicken during the re-melting process, which leads to an overall decrease of the Al content in the remaining coating material. Based on the measured thickness of the intermetallic layer, the composition of re-solidified coatings could be estimated at Al–51 wt.% Zn–1.6 wt.% Si. The liquidus temperature for this alloy composition is 547 °C. Solidification at 532 °C corresponds to an undercooling of 15 K and to a supersaturation of 0.21 [17].

4. Discussion

In this section three different mechanisms potentially responsible for the formation of intragranular misorientations are discussed in the light of the above described experimental findings. The first mechanism is the thermomechanical hypothesis that has been suggested by Sémoroz and coworkers [1] and which has already been briefly presented in the introduction. The re-solidification experiments conducted with the thermal contraction modified by the brass support indicate that the thermomechanical stresses do not significantly influence the intragranular misorientations. One could argue that the thermal strain is not completely eliminated as the expansion coefficient of brass (21.4×10^{-6} K^{-1}), in spite of being considerably larger than that of steel (12×10^{-6} K^{-1}), is not exactly as high as in the Al–Zn–Si alloy (23.5×10^{-6} K^{-1}). However, there is no doubt that the plastic strain state in the coating was considerably modified by the presence of the brass support, without inducing any relevant change in the misorientation distribution.

Another argument against the thermomechanical hypothesis is the continuous character of the orientation change, which is systematically observed along the dendrite arms. This feature of the misorientations distribution suggests that misorientations develop during dendritic growth rather than after solidification. The cooling curves measured in the re-solidification experiments (Fig. 6) indicate that the dendrite network expands during very small time and temperature intervals. It can indeed be assumed that,

at a volume fraction of solid of about 1/3, the expansion of the dendritic network is almost finished and solidification then proceeds mainly by thickening of existing dendrites arms until eutectic is formed. As a consequence, the differential thermal contraction between the substrate and the coating during the expansion of the dendritic network can be neglected as the temperature interval is very small (about 3 K). If one considers only the thermomechanical hypothesis, continuous variations of the crystallographic orientation would have no reason to develop during the expansion of the dendritic network. Successive "bending" events of the dendrite arms during growth, as illustrated in Fig. 7a, must therefore be excluded under the thermomechanical hypothesis. Consequently, misorientations would have to be the result of plastic deformation after dendritic growth. Plastic deformation would lead to crystal rotations as illustrated in Fig. 7b, where the local rotation angle with respect to the original orientation would strongly depend on the position in the grain. This seems implausible since the driving force supposedly responsible for the formation of misorientations, the thermal strain, is in principle uniform throughout the grains.

A second mechanism to take into consideration is the microsegregation hypothesis which was also suggested by Sémoroz et al. [1]. It postulates that the misorientations observed in Al–Zn–Si hot-dip coatings may be due to microsegregation, which leads to systematic concentration gradients across the coating thickness. These gradients would lead to crystal distortions generated by the variations of the lattice parameter. In order to produce the observed misorientation pattern, where the crystal lattice has always a convex shape (the crystal rotates towards the substrate as one moves from the nucleation centre to the grain boundary), the Zn concentration needs to increase monotonically from the free surface to the substrate. This condition is, however, not verified by the microsegregation profiles obtained by GD-OES, which show that the Zn tends to segregate in the centre of the coating rather than near the substrate (Fig. 4). Another argument against the microsegregation hypothesis is the fact that pronounced misorientations have also been observed in very dilute Zn–Al alloys where microsegregation is very limited [13]. A more detailed discussion of the thermomechanical and microsegregation hypotheses has been reported elsewhere [15].

As thermal stresses and microsegregation can be dismissed as dominant mechanisms for the formation of misorientations in Al–Zn–Si coatings, a new hypothesis is proposed here. This mechanism is related to the solidification shrinkage and the proximity of the free surface. In the solidification of bulk samples, the shrinkage is compensated by an inflow of liquid metal antiparallel to the moving direction of the grain envelope. Depending on the solidification velocity and the size of the casting, this can lead to a transport of liquid over considerable distances. In thin coatings the situation is considerably different as the solidification shrinkage is easily compensated by lowering the level of the liquid metal in the coating, which is associated with a liquid flow approximately perpendicular to the growth direction of the dendritic front. The solidification shrinkage is responsible for the formation of the surface topography observed in Fig. 5, where the surface level is tightly correlated with the dendritic pattern. If the dendrite tips grow close to the free surface, a decrease of the surface level will occur only in between the dendrite arms. This leads to a curved liquid–air interface, which is inclined at the triple junction between solid, liquid and air, as illustrated in Fig. 8. The AFM measurements of Fig. 5b shows the presence of an oxide skin at the surface of the coating. The formation of the surface topography during dendritic growth corresponds to an increase of the surface area, which is associated with a tensile straining of the oxide film. The stress state in strained oxide films on Al melts has been studied by Syvertsen, who found that the yield tension of the oxide skin is about $\gamma = 0.72\ \mathrm{N\ m^{-1}}$ for many Al-based alloys [18]. This tension applies in the triple junction between solid, liquid and air (Fig. 8). In the presence of an inclination at the triple junction, η, a vertical force, $F_z = \gamma \sin \eta$, acts on the contour of the dendrite arm.

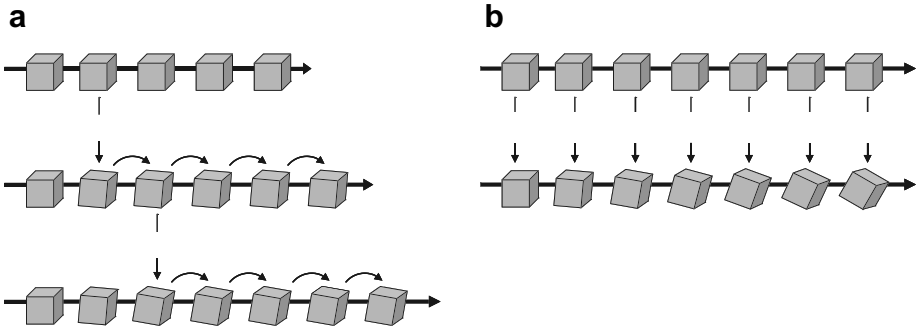

Fig. 7. Schematic representation of possible mechanisms leading to a continuous variation of the crystal orientation along a dendrite trunk, assuming a constant misorientation rate and a rotation axis perpendicular to the dendrite arm. If misorientations develop during growth, continuous misorientations can be obtained by repeated bending events (a), whereas the rotation angle must increase with the distance from the nucleus if misorientations develop after growth (b).

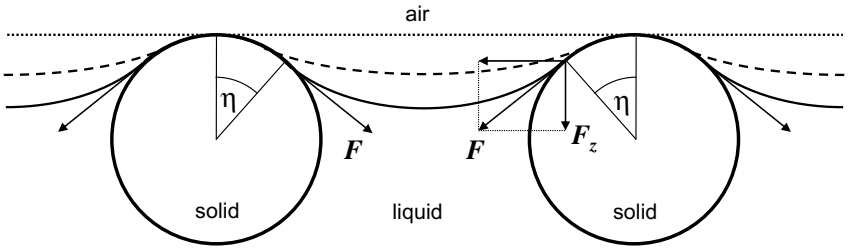

Fig. 8. Schematic cross-section through two dendrite arms growing at the surface of the coating. The solidification shrinkage leads to a depression of the melt level and to an increasingly curved liquid–air interface, which is schematically shown by the transition from the dotted line, to the dashed and solid lines.

In order to get a realistic estimate of the inclination η, one can refer to the topography profiles taken on the surface of Al–Zn–Si coatings. Once the oxide skin comes into contact with the dendrite arm, one can assume that the shape of the "emerged" part of the dendrite arm no longer changes and that the inclination of the surface will remain constant. Therefore, topography profiles can be considered as trajectories of triple junctions. A relationship between the liquid level and the inclination η was established based on the AFM profile of Fig. 9, which corresponds to the black line drawn in Fig. 5. It was assumed that the straight line connecting the tops of the humps in Fig. 9 corresponds to the level of the molten layer prior to solidification and that the shrinkage volume ΔV at a certain stage of solidification is given by the grey volume illustrated in Fig. 9. By averaging η on several dendrite humps, a mean inclination could be determined for a given ΔV. The latter quantity is obtained by numerical integration of the AFM profile.

The inclination of the triple junction prevailing during the development of the dendritic network can now be estimated if the amount of solidification shrinkage is known. The solidification shrinkage accumulated during the development of the dendritic network is directly related to the proportion of solid contained in the dendritic grains during their expansion. This quantity should be in any case lower than the volume fraction of solid that was determined for the end of the inflection in the cooling curve of Fig. 6 (estimated at 0.33), since this moment was associated with the end of the dendritic network extension. As the liquid within the grain envelopes is certainly well-mixed, the proportion of solid within the dendritic grain can be considered as approximately equal to the supersaturation. As seen above, this quantity can be estimated to be about 0.2. If a total solidification shrinkage of 5.5% is considered, which is typical for this type of coating alloys [15], the shrinkage at the grain envelope would then be 1.16%. In further calculations a 1% shrinkage across the grain envelope is used. Knowing the thickness of the coating, the relative shrinkage can be converted into an absolute volume shrinkage ΔV which is then used to estimate the inclination at the triple junction, η, according to the above-explained procedure. A relative shrinkage of 1% yields an inclination $\eta = 17°$ and a vertical force, $F_z = \gamma \sin\eta = 0.21\ \mathrm{N\,m^{-1}}$, acting on the contour of the dendrite arm.

In order to estimate the mechanical response of a dendrite arm, the dendrite contour on which the vertical force F_z applies needs to be known. It is considered that the vertical force mainly acts in the area where substantial solidification shrinkage occurs and where the oxide skin is strained in tension. The size of this region has been assessed by phase field simulation. The simulations were performed in 2D and using the model of Tiaden et al. [19]. The details of the calculation were reported elsewhere [15]. Fig. 10a shows the contour of a dendrite arm obtained by phase field simulation for Al–44 wt.% Zn solidifying at 550 °C. This dendrite exhibits a trunk radius of about 2.2 μm, which is in good agreement with the WDS analysis of the dendritic pattern that is shown in Fig. 10b. This WDS analysis was performed in an as-received sample and in a cross-section that is almost parallel to a primary arm.

The phase field simulation shows also that the largest solidification rate and hence solidification shrinkage occurs in a zone of about 40 μm behind the envelope formed by the dendrite tips. By integrating the vertical force F_z over

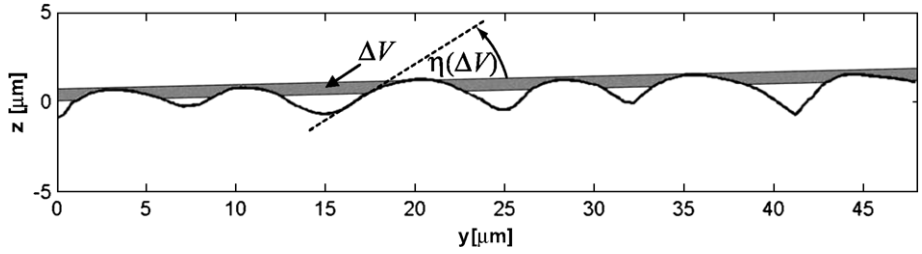

Fig. 9. Schematic illustration of the method used to determine the relationship between the solidification shrinkage ΔV and the inclination η of the coating surface.

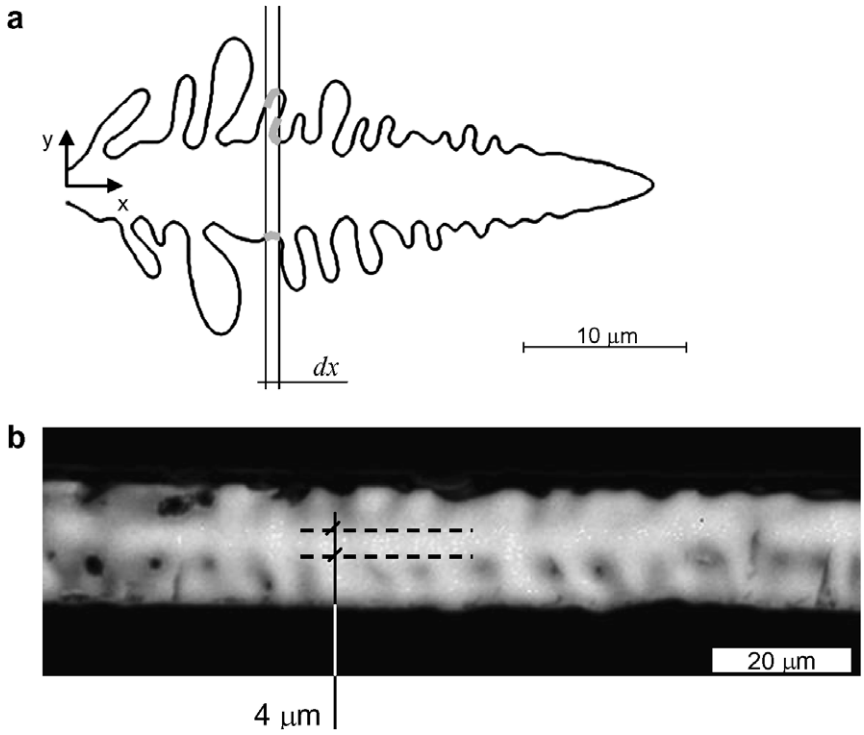

Fig. 10. (a) Contour of a dendrite arm growing into the supersaturated melt determined by phase field simulation. The contour length per unit distance ds/dx is given by the length of all the contour segments (in grey) falling into a given distance increment dx. (b) WDS intensity map of the K_α Al peak in a cross section taken almost parallel to a primary dendrite arm in the centre of the coating layer.

the contour, the bending moment along the dendrite arm, $M_y(x)$, can be obtained:

$$M_y(x) = -F_z \int_x^{x_{\text{tip}}} \int_{\xi_1}^{x_{\text{tip}}} \frac{\mathrm{d}s}{\mathrm{d}x}(\xi_2)\mathrm{d}\xi_2\,\mathrm{d}\xi_1 \tag{2}$$

where ξ_1 and ξ_2 are auxiliary integration variables and $\frac{\mathrm{d}s}{\mathrm{d}x}(x)$ is a function describing the length of the segments of the dendrite contour as a function of x. For the dendrite geometry shown in Fig. 10a, a maximum bending moment of $M_y(x=0) = -6 \times 10^{-10}$ N m is reached. The stress distribution in the dendrite arm can now be estimated if one considers a purely elastic response:

$$\sigma_{xx} = -z\frac{M_y}{I_{yy}} \tag{3}$$

where I_{yy} is the second moment of area around the neutral axis and z is the distance from the neutral axis.

If dendrite arms are assumed to have a circular cross-section of a radius $r_\mathrm{d} = 2.5$ μm, the second moment is then given by $I_{yy} = \pi r_\mathrm{d}^4/4 \cong 3 \times 10^{-23}$ m^4. The stress can therefore be as high as 50 MPa at the surface of the dendrite.

Unfortunately, there are no literature data of the mechanical properties of the Al–Zn–Si crystals at the temperature of interest (~530 °C). However, the mechanical behaviour of other Al-based alloys at high temperature has been reported in literature [20–22]. They show an elastic–perfectly plastic behaviour with yield stresses that depend on the strain rates but are significantly lower than the above-mentioned threshold of 50 MPa. In addition the assumption of a 5 μm diameter is realistic but rather conservative since phase field simulations show dendrite necks exhibiting substantially lower diameters. Therefore, it can perfectly be envisaged that dendrite arms are plastically bent by the effect of the surface tension (or oxide skin resistance) associated with the creation of a surface topography due to solidification shrinkage.

Plastic deformation occurs by the multiplication and movement of dislocations. Following the reasoning of Motz et al. [23], the movement of dislocations under the effect of a bending moment can lead to the accumulation of geometrically necessary dislocations (GNDs) and hence to variations of the crystallographic orientation. Dislocation sources such as Frank–Read sources emit dislocation dipoles or loops. In the presence of shear stress, the dislocations of a dipole move away from each other. One of them moves towards the solid–liquid interface where it is annihilated, while the other one moves towards the centre of the dendrite arm, where the shear stress changes sign. As a result, dislocations of one sign pile up in the central region of the dendrite arm, corresponding therefore to the creation of GNDs associated to a variation of the crystallographic orientation. The vertical component of the force in the oxide film, which applies on the contour of the dendrite arm, leads to a bending moment oriented towards the substrate, say downwards. As the stress state is tensile in the upper part of the dendrite arms and compressive in the lower part, dislocations having a component of their excess atomic plane upwards move towards the

centre of the dendrite arms. Dislocations having their excess atomic plane downwards are annihilated at the solid–liquid interface. The resulting accumulation of GNDs corresponds to a rotation of the crystal orientation towards the substrate. This is in good agreement with the EBSD observations, which reveal a systematic and cumulative rotation of the crystal lattice around an axis lying in the coating plane and about perpendicular to the growth direction. It was observed also that the misorientations can either be completely continuous or concentrated in dendrite necks. These two observations correspond to misorientation types 1 and 2 in Fig. 1b, respectively. Both situations are consistent with the mechanism proposed here, as misorientations and GNDs are likely to be more concentrated in branching necks due to the increased stress level in the thinnest sections of the dendritic network.

5. Conclusion

The present investigation provides new insight into the formation of solidification microstructures in Al–Zn–Si hot-dip coatings and the origin of intragranular crystallographic misorientations. The main outcomes can be summarized as follows:

- During solidification of industrial hot-dip Al–Zn–Si coating the dendrite network forms at high supersaturation and growth rates. As a consequence the internal solid fraction of the dendritic grain is high (typically 0.33) and a substantial increase of the volume fraction of solid occurs just behind the envelope of the growing grain.
- The solidification shrinkage is compensated by a decrease of the melt level in between the dendrite arms. It leads a surface topography and wrinkles in the oxide skin, which were clearly revealed by AFM.
- As GD-OES analyses did not reveal a significant Zn accumulation near the substrate, the intragranular crystallographic misorientations observed in the Al–Zn–Si coatings are not due to microsegregation. The hypothesis of thermomechanical stresses due to differential thermal contraction between the substrate and coating is also ruled out as a possible origin of intragranular misorientations, since it is not consistent with the observed orientation distribution in as-received and re-solidified specimens.
- As a new hypothesis, it is proposed that the solidification shrinkage is the driving force for the formation of intragranular misorientations. The solidification shrinkage leads to an increase of the surface roughness and hence of the surface area of the coating. Therefore, tensile stresses develop in the oxide skin spanning the surface of the melt. They translate into forces that apply on the dendrite network. It was shown that the resulting bending moment is sufficient to deform plastically the dendrite arms, introducing thereby the geometrically necessary dislocations for the variation of the crystallographic orientation.

The new mechanism that is proposed here for crystallographic misorientations in hot-dip coatings requires a large contact area between the dendritic network and the free surface. The mechanism is therefore not directly applicable to the misorientations observed in bulk materials such as cast Ni-based alloy components. The present analysis confirms however that plastic deformation of a dendritic network is relatively easy to achieve during solidification. It is therefore expected to prevail in other systems where intragranular misorientations are also observed after solidification.

Acknowledgements

The authors would like to acknowledge the research commissions of the Ecole Polytechnique Fédérale de Lausanne (EPFL), Switzerland, and of the Swiss Federal Institute for Materials Testing (EMPA), Switzerland, for their financial support.

References

[1] Sémoroz A, Durandet Y, Rappaz M. Acta Mater 2001;49:529.
[2] Rappaz M, Blank E, Cryst J. Growth 1986;74:67.
[3] Agapova EV, Pankin GN, Ponomarev VV, Larionov VN, Denisov AY. Izvestiya Akademii Nauk SSSR. Metally 1989;2:104.
[4] Paul U, Sahm PR, Goldschmidt D. Mater Sci Eng A 1993;173:49.
[5] Siredey N, Boufoussi M, Denis S, Lacaze J, Cryst J. Growth 1993;130:132.
[6] Napolitano RE, Schaefer RJ. J Mater Sci 2000;35:1641.
[7] Newell M, Devendra M, Jennings PA, D'Souza N. Mater Sci Eng A 2005;412:307.
[8] D'Souza N, Newell M, Devendra K, Jennings PA, Ardakani MG, Shollock BA. Mater Sci Eng A 2005;567:413–4.
[9] Wagner A, Shollock BA, McLean M. Mater Sci Eng A 2004;374:270.
[10] Agapova EV, Tagirova DM, Gundyrev VM. Phys Met Metall 1997;84:171.
[11] Mullis AM, Walker DJ, Battersby SE, Cochrane RF. Mater Sci Eng A 2001;245:304–6.
[12] Dragnevski K, Mullis AM, Walker DJ, Cochrane RF. Acta Mater 2002;50:3743.
[13] Sémoroz A. PhD thesis, EPFL, Lausanne; 2001.
[14] Payling R, Michler J, Aeberhard M. Surf Interf Anal 2002;33:472.
[15] Ch. Niederberger, PhD thesis, EPFL, No. 3863, Lausanne; 2007.
[16] Niederberger C, Michler J, Jacot A. In: Gandin C-A, Bellet M, editors. Modeling of casting, welding and advanced solidification processes, vol. XI. Warrendale, PA: TMS; 2006. p. 481.
[17] Thermo-Calc software, Stockholm, and Al-Data database of Sente Software Ltd., Surrey Technology Centre, UK.
[18] Syvertsen M. Metall Mater Trans B 2006;37:495.
[19] Tiaden J, Nestler B, Diepers HJ, Steinbach I. Physica D 1998;115:73.
[20] Van Haaften WM, Magnin B, Kool WH, Katgerman L. Metall Mater Trans A 2002;33:1971.
[21] Ludwig O, Drezet J-M, Martin CL, Suery M. Metall Mater Trans A 2005;36:1525.
[22] Ludwig O, Drezet J-M, Ménésès P, Martin CL, Suery M. Mater Sci Eng A 2005;174:413–4.
[23] Motz C, Schöberl T, Pippan R. Acta Mater 2005;53:4269.